Ordered Nanopillar Structured Electrodes for Depleted Bulk Heterojunction Colloidal Quantum Dot Solar Cells

11 AUTHORS, INCLUDING:

Illan J Kramer
University of Toronto
32 PUBLICATIONS **1,585** CITATIONS

SEE PROFILE

Philip M Rice
IBM
109 PUBLICATIONS **6,848** CITATIONS

SEE PROFILE

Ratan Debnath
National Institute of Standards and Techno…
55 PUBLICATIONS **2,500** CITATIONS

SEE PROFILE

Edward H Sargent
University of Toronto
416 PUBLICATIONS **13,498** CITATIONS

SEE PROFILE

Ordered Nanopillar Structured Electrodes for Depleted Bulk Heterojunction Colloidal Quantum Dot Solar Cells

Illan J. Kramer, David Zhitomirsky, John D. Bass, Philip M. Rice, Teya Topuria, Leslie Krupp, Susanna M. Thon, Alexander H. Ip, Ratan Debnath, Ho-Cheol Kim,* and Edward H. Sargent*

Colloidal quantum dots (CQDs) have shown great promise in recent years as the active material[1] in third generation photovoltaic devices.[2] In particular, the development of the depleted-heterojunction solar cell[3] has enabled power conversion efficiencies (η) to reach 6%.[4] Despite progress in performance, there still exists a compromise between the absorption of light (where films approaching 1 μm are required to absorb all incident above-bandgap photons[5]) and the extraction of current (where a diffusion length on the order of 10 nm is characteristic of CQD films[6] and depletion is typically limited to 100–200 nm[3]).

Materials and device architecture can play an important role in breaking this compromise. Recent reports have demonstrated performance enhancements through landscaping the *energetic* profile of the quantum dot film through the deployment of a quantum funnel[7] as well as the *geometric* profile through a textured porous electrode.[8] This second method allows for collection of charge carriers that would otherwise recombine within the quasi-neutral region if a planar geometry were employed. This device, known as a depleted bulk heterojunction (DBH), is the CQD analogue of bulk heterojunctions widely deployed, to beneficial effect, in organic photovoltaics.[9] The DBH has been implemented both with ZnO nanowires[10] and large TiO$_2$ nanoparticles[8] as the electron-accepting template into which CQDs are deposited. A three-dimensionally-configured depletion region allows the incorporation of more CQD material for more complete light absorption while maintaining efficient charge collection.[8]

To date, disordered structured electrodes have been employed, such as those based on polydispersed nanoparticle titania. This produces both voids and islands, compromising the advantages of the DBH strategy.

Here we present a novel, ordered structured electrode and deploy it in the realization of infrared-bandgap depleted-heterojunction CQD solar cells. In view of their size-tunability and infrared bandgap, we employ PbS CQDs. We provide titania nanopillars, having a defined spacing, height, and aspect ratio, that lead to enhanced charge collection. We employ a transfer molding technique that enables large areas of uniform topography defined via a master template.[11] The nanopillars are arranged in a hexagonal pattern wherein each nanopillar is equidistant from its nearest neighbours at a peak-to-peak distance of approximately 275 nm as seen in **Figure 1**.
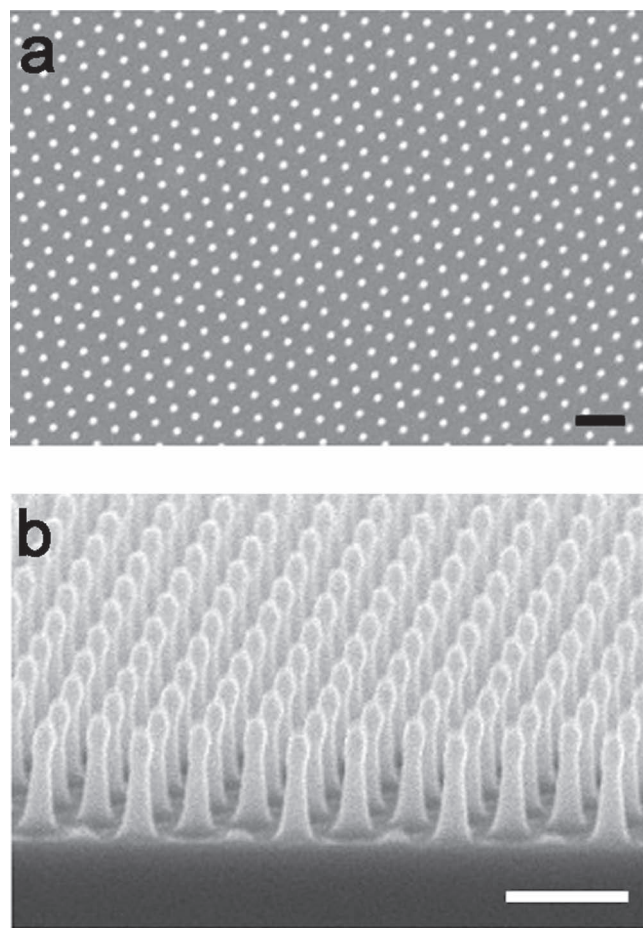
Figure 1. SEM images of a) top and b) angled side views of titania nanopillars on FTO-coated glass substrates. The hexagonal orientation of the nanopillar array results in sets of equilateral triangles ensuring ~275 nm spacing between nearest neighbours. The scale bars are 500 nm.

I. J. Kramer,[+] D. Zhitomirsky,[+] Dr. S. M. Thon,
A. H. Ip, Dr. R. Debnath, Prof. E. H. Sargent
Department of Electrical and Computer Engineering
University of Toronto
10 King's College Road, Toronto, Ontario M5S 3G4, Canada
E-mail: ted.sargent@utoronto.ca
Dr. J. D. Bass, Dr. P. M. Rice, Dr. T. Topuria, L. Krupp, Dr. H.-C. Kim
IBM Research Division
Almaden Research Center
650 Harry Road, San Jose, CA 95120-6099, USA
E-mail: hckim@us.ibm.com
[+] I.J.K and D.Z. contributed equally to this work.

© 2012 WILEY-VCH Verlag GmbH & Co. KGaA, Weinheim
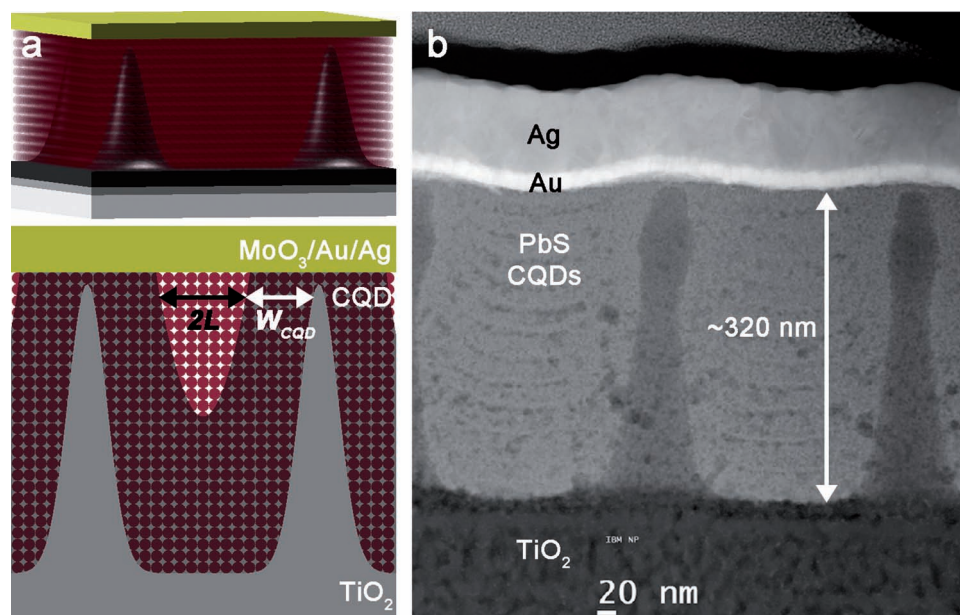
Figure 2. a) Cartoon depiction and b) Z-contrast STEM images of fabricated solar cells. Individual layers of CQD formed by the layer-by-layer process can clearly be seen. Also evident is the minimization of separation between the nanopillar and back contact. The MoO₃ layer is very thin (10 nm) and falls between the PbS CQD layer and the Au layer.

We optimized the nanopillar spacing based on measurements indicating a ~150–200 nm depletion region in the best CQD films reported to date.[3] To collect photogenerated carriers efficiently, the distance between adjacent nanopillars must follow Equation 1:

$$d_{np-np} \approx 2 \cdot \left(W_{CQD} + L \right) \qquad (1)$$

where d_{np-np} is the distance between adjacent nanopillars, W_{CQD} is the portion of the depletion width residing in the CQD film and L is the diffusion length of minority carriers (*i.e.* electrons) in the CQD film. By spacing the nanopillars at 275 nm, Equation 1 is satisfied, ensuring that all photogenerated electrons will be generated in or very near to a depletion region. d_{np-np} is an upper bound on collection length; it is desirable to array nanopillars at or near this spacing to maximize the volume fill fraction of the light-absorbing CQDs.

CQDs were deposited in a layer-by-layer fashion until a desired thickness was reached. This thickness, for such a three-dimensional bulk heterojunction, must be slightly greater than the height of the nanopillars themselves to avoid direct contact between the top ohmic contact and the TiO₂. MoO₃ followed by gold/silver was used to ensure an ohmic characteristic.[12,13] We depict this design and its realization in **Figures 2**a and 2b.

Figures 3a and 3b show cross-sectional TEM images of the fabricated planar and nanopillar devices, demonstrating the bicontinuous nature of the CQD/TiO₂ interface. In Figure 3b, the thin layer of CQDs separating the tops of the TiO₂ nanopillars from the MoO₃/Au/Ag contacts is evident. Also visible is a thick planar layer of TiO₂ nanograins beneath the CQD layer arising from the use of a titanium n-butoxide based sol-gel approach,[14] the titania layer prepared using an acetylacetone chelated organotitanate. n-Butyl polytitanate (Tyzor BTP, DuPont) was reacted with acetylacetone to synthesize the chelated titanate. The solution was diluted with propylene glycol propyl ether (PGPE). The organotitanate solution was spin-coated on clean FTO substrates and subsequently baked at 450 °C for 2 hours to crystallize the titanate. This gives a flat anatase titania layer on FTO which contains polycrystalline
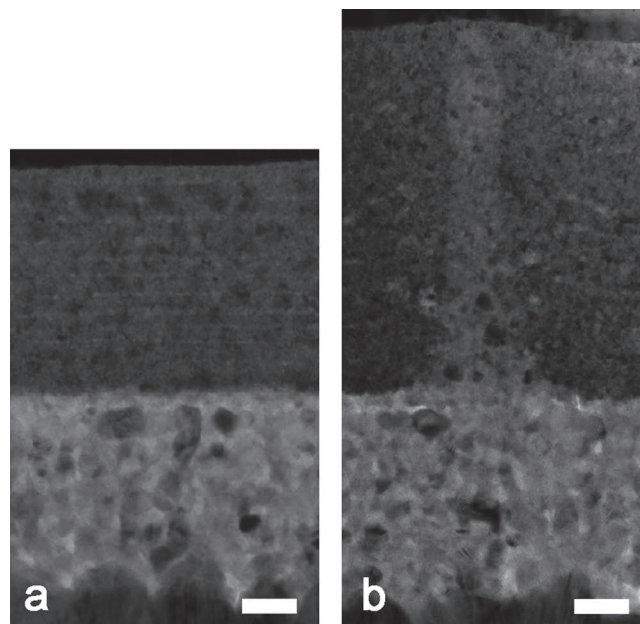

Figure 3. Cross-sectional TEM images of a) planar and b) nanopillar fabricated devices using 13 layers of CQDs. The scale bars are 50 nm. Nanopillars enable thicker layers of CQDs to deposit within a single deposition cycle.

titania of approximately 10 nm grain size as seen in Figures 3a and 3b.[15]

Figures 4a shows the forward (i.e., open-circuit (OC) to short-circuit (SC), black curves) and reverse (i.e., SC to OC, grey curves) current density vs. voltage (*J–V*) performance of the planar and nanopillar samples. We provide external quantum efficiency and absorption spectra for both planar and nanopillar samples in Figure 4b.
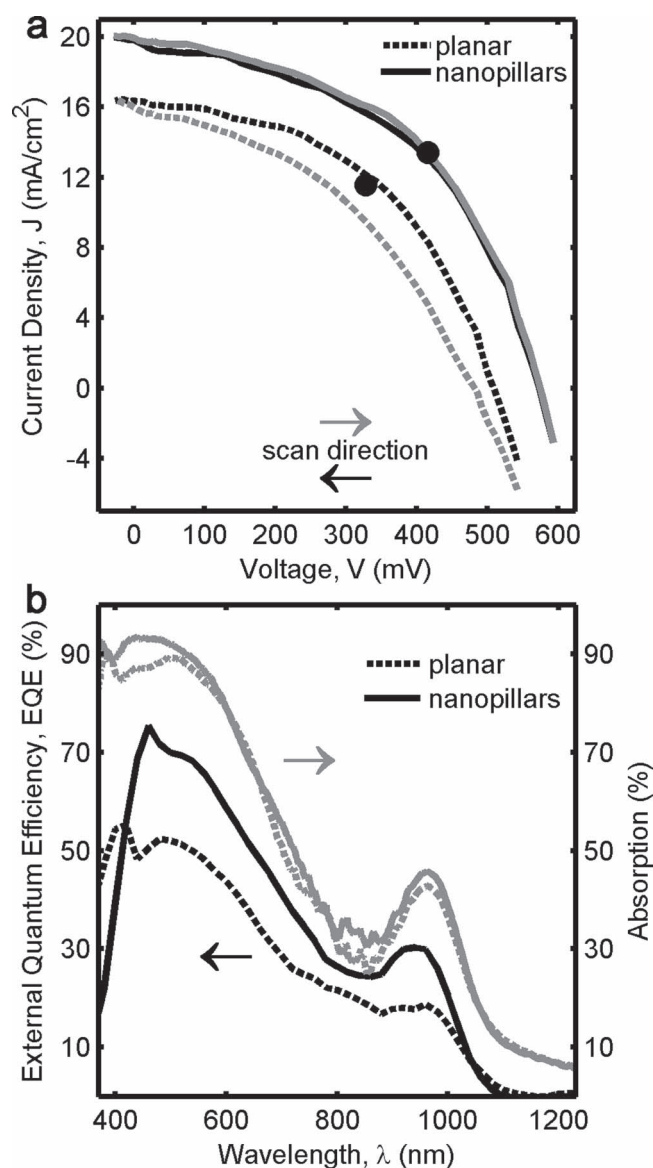

Figure 4. a) *J–V* curves under AM 1.5 illumination of planar and nanopillar devices showing $\eta = 5.6\%$ for the nanopillar architecture. The black curves represent the forward scan (*i.e.* from OC to SC), while the grey curves represent the reverse scan taken immediately after the forward scan (*i.e.* from SC to OC). The black circles represent the static current measured at the maximum power point, confirming the $\eta = 5.6\%$ performance. b) EQE (black) and absorption (grey) curves of the devices represented in figure a). Clearly the nanopillar architecture benefits from enhanced collection despite having nearly identical absorption as the planar counterpart.

The nanopillar device exhibits a much higher open-circuit voltage, V_{OC}, than both the planar control and the previously published depleted bulk heterojunction results.[8,10] Since traps – both interfacial and in the CQD film bulk - can lead to Fermi level pinning,[16] they constrain the V_{OC} attainable in the device. Since the CQD/TiO$_2$ interface has a larger surface area in the nanopillar case compared to the planar, the fact that nanopillars achieve a notably higher V_{OC} indicates that traps in the bulk of the CQD films are the performance-limiting mechanism[17] in these devices, instead of titania-CQD interfacial traps. Charge collection by nanopillars competes successfully against capture of photocarriers to traps in the quantum dot film, a fact that helps both V_{OC} and short-circuit current density, J_{SC}. Very low hysteresis in the nanopillar sample further confirms that collection wins over trapping.[18,19]

We turned to self-consistent two-dimensional optoelectronic modelling to explore systematically the conditions to achieve a performance enhancement using the structured electrode. **Figures 5**a and 5b illustrate optoelectronic modelling results for the electric field at the operating voltage (i.e. the maximum power point) for the case of a planar *versus* nanopillar architecture. In the nanopillar case, the electric field is stronger in the volume surrounding the nanopillars, thereby increasing the volume from which photogenerated carriers can be extracted. The model posits traps of depth 0.25 eV below the conduction band edge[20] that serve to limit the separation of the quasi-Fermi levels under solar illumination as well as impede transport of free carriers.[21] To explore further the causes of enhanced carrier extraction, we inspected trap occupation probabilities (Figures 5c and 5d) as well as Shockley-Reed-Hall (SRH) recombination rates (Figures 5e and 5f) for the planar and nanopillar cases. The nanopillars enhance carrier extraction by ensuring that more photocarriers see efficient field-driven transport that overcomes recombination. Similar nanopillar-enabled suppression of SRH recombination has been seen previously in electro-optical models of organic nanopillar photovoltaics.[22] Electro-optical modelling parameters are outlined in SOM 1.

Table 1 summarizes the figures of merit extracted from the *J–V* curves of Figure 4a. Static V_{OC}, J_{SC} and maximum power point measurements are also included that confirm the $\eta = 5.6\%$ measured during the *J–V* scan. The static J_{SC} value of 19 mA/cm^2 achieved by the nanopillar samples is similar to the J_{SC} previously reported using infiltration of colloidal quantum dots into much thicker TiO$_2$ nanoparticle layers.[8] The nanopillar sample, unlike the large TiO$_2$ nanoparticle sample, is limited in the vertical direction by the height of the nanopillars. Because of this limitation, the 320 nm film absorbs only 46% of incident light at the exciton wavelength (Figure 4b), whereas the much taller TiO$_2$ nanoparticle device showed >60% absorption at the exciton wavelength. Despite the reduction in long-wavelength absorption, the nanopillar device exhibits similar extracted current and overall enhanced power conversion efficiency.

While CQD materials continue to improve, leading to further progress in optical and electrical properties, solar cell device architecture remains critical in achieving high efficiencies. By tailoring the bulk heterojunction concept to the transport characteristics of CQD films, we enhanced charge collection efficiency in three dimensions. Using conveniently

COMMUNICATION
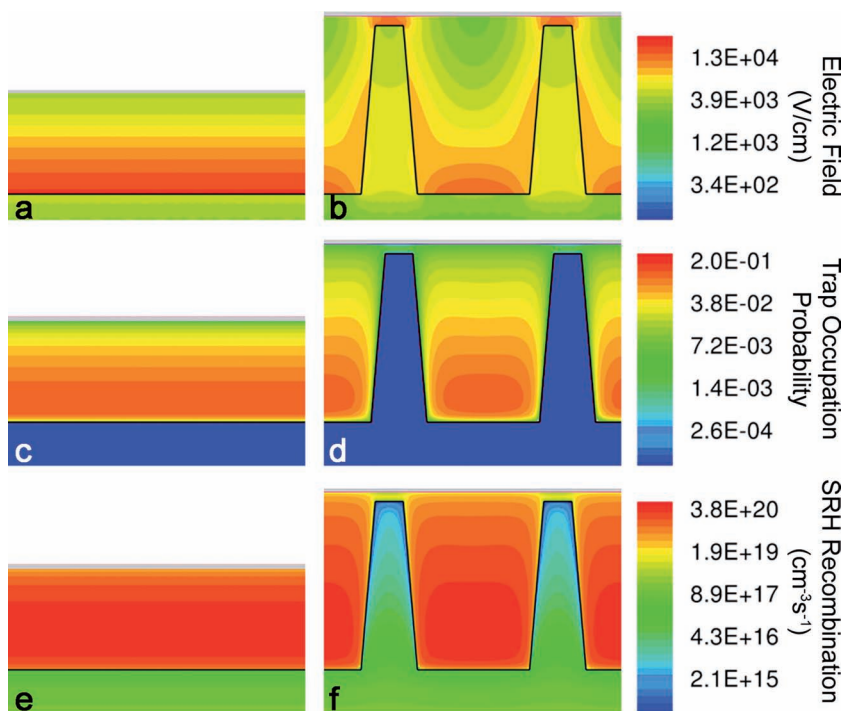
Figure 5. Electric field distributions in a) planar and b) nanopillar devices indicating that carriers generated deeper in the device will still encounter the charge-extracting field. Trap occupation (c and d) and SRH recombination (e and f) of planar (c and e) and nanopillar (d and f) architectures indicating how trap filling and therefore trap-related recombination is suppressed in the volumetric vicinity of the nanopillars.

available patterning technologies, we showed that, with this optimal template design, power conversion efficiencies of 5.6% can be achieved using available PbS CQD films–efficiencies that exceed those achieved using planar electrode approaches.

Table 1. Figures of merit for planar and nanopillar devices. Static values were recorded for V_{OC}, J_{SC} and the maximum power point and are reported along with voltage sweeps from open-circuit to short-circuit as well as from short-circuit to open-circuit.

Parameter		Units	Planar	Nanopillar
Static	V_{OC}	mV	520	570
	J_{SC}	mA/cm^2	16.1	19.0
	η	%	3.8	5.6
Open-Circuit → Short-Circuit	V_{OC}	mV	500	570
	J_{SC}	mA/cm^2	16.4	19.7
	FF	%	49	49
	η	%	4.1	5.5
	R_S	$\Omega \cdot$cm^2	9.7	7.1
Short-Circuit → Open-Circuit	V_{OC}	mV	490	580
	J_{SC}	mA/cm^2	16.2	20.1
	FF	%	41	49
	η	%	3.2	5.7
	R_S	$\Omega \cdot$cm^2	11.9	6.2

Experimental Section

Titania Nanopillar Fabrication: Titania structure was prepared using an acetylacetone chelated organotitanate. n-Butyl polytitanate (Tyzor BTP, DuPont) was reacted with acetylacetone to synthesize the chelated titanate. The solution was diluted with propylene glycol propyl ether (PGPE). The organotitanate solution was spin-coated on clean FTO substrates and subsequently baked at 450 °C for 2 h to crystallize the titanate. This gives a flat anatase titania layer on FTO which contains polycrystalline titania of approximately 10 nm in grain size. Titania nanopillars were fabricated using a transfer molding technique using a water soluble polymer template. The polymer template was prepared by molding a poly(vinyl alcohol) (PVA) on a silicon master which contains pillars of ~135 nm in diameter at half-height, 750 nm tall and a 275 nm center-to-center spacing. The silicon master was prepared using conventional optical lithography and plasma etching. Acetic acid was added to the PGPE solution of the organotitanate and the solution was spin-coated onto a PVA daughter template at 2000 rpm for 45 s. The sample was heated to 80 °C for 10 s before transfer onto the titania coated FTO substrates. The sample was exposed to 245 nm UV illumination at room temperature for 30 min. Dissolution of the PVA template was carried out at 42–85 °C (pH 4–7) for 25 min. The film was rinsed with water then dried with ethanol and nitrogen before the calcination of titania was carried out by baking at 450 °C for 2 h (ramp up at 5 °C/min).

CQD Synthesis: PbS colloidal quantum dots were synthesized using a variation on a literature method[23] consistent with our previous CQD solar cells.[4]

Device Fabrication: CQD films were prepared on nanopillar electrodes by multilayer spincoating of 37.5 mg mL^{-1} solution in octane under ambient conditions. Each layer was deposited at 2500 rpm and treated briefly with 1% 3-mercaptopropionic acid in methanol also spin cast at 2500 rpm; each layer was then rinsed with methanol and octane while spinning at 2500 rpm. The device was then transferred to a glovebox with N$_2$ atmosphere and left overnight. Contacts consisting of 10 nm of MoO$_3$, topped with 50 nm of gold and 80 nm of silver were deposited by thermal and electron beam evaporation at a rate of 0.2 (thermal), 0.4 (electron beam) and 1 Å/s (thermal), respectively, at a pressure of <1 × 10^{-6} mbar. Contact sizes were 0.061 cm^2.

J–V Characterization: J–V data was measured using a Keithley 2400 source-meter under ambient conditions. The solar spectrum at AM1.5 was simulated to within class A specifications (less than 25% spectral mismatch) with a Xe lamp and filters (ScienceTech) with measured intensity at 100.4 mW cm^2. The source intensity was measured with a Melles-Griot broadband power meter (responsive from 300 to 2000 nm), through a circular 0.049 cm^2 aperture at the position of the sample and confirmed with a calibrated solar cell (Newport, Inc.). The aperture is smaller than the contact size to ensure that there is no lateral current collection. This is done to minimize any device-size effects. The accuracy of J–V measurements was estimated to be ±7%.

Electron Microscopy: SEM was performed on a Htachi S-4700 at 3 kV. For TEM analysis, ~50 nm thick cross sectional slice containing nanopillars was prepared using focus ion beam (FIB). Specimen's surface was coated with carbon, e-beam and ion beam platinum prior to TEM sample preparation for protection. Conventional TEM and High Angle Annular Dark field (HAADF) STEM images were acquired using a JEOL 2010F.

Absorption Measurements: Absorption spectroscopy was carried out using a Cary 500 UV-vis-IR Scan photospectrometer with an attached integrating sphere.

Supporting Information

Supporting Information is available from the Wiley Online Library or from the author.

Acknowledgements

[1] E. H. Sargent, *Nat. Photon.* **2009**, *3*, 325–331.

[2] M. A. Green, *Third Generation Photovoltaics: Advanced Solar Energy Conversion*, Springer-verlag. **2006**.

[3] A. G. Pattantyus-Abraham, I. J. Kramer, A. R. Barkhouse, X. Wang, G. Konstantatos, R. Debnath, L. Levina, I. Raabe, M. K. Nazeeruddin, M. Gratzel, E. H. Sargent, *ACS Nano* **2010**, *4*, 3374–3380.

[4] J. Tang, K. W. Kemp, S. Hoogland, K. S. Jeong, H. Liu, L. Levina, M. Furukawa, X. Wang, R. Debnath, D. Cha, K. W. Chou, A. Fischer, A. Amassian, J. B. Asbury, E. H. Sargent, *Nat. Mater.* **2011**, *10*, 765–771.

[5] D. A. R. Barkhouse, I. J. Kramer, X. Wang, E. H. Sargent, *Opt. Express* **2010**, *18*, A451–A457.

[6] K. W. Johnston, A. G. Pattantyus-Abraham, J. P. Clifford, S. H. Myrskog, S. Hoogland, H. Shukla, E. J. D. Klem, L. Levina, E. H. Sargent, *Appl. Phys. Lett.* **2008**, *92*, 122111.

[7] I. J. Kramer, L. Levina, R. Debnath, D. Zhitomirsky, E. H. Sargent, *Nano Lett.* **2011**, *11*, 3701–3706.

[8] D. A. R. Barkhouse, R. Debnath, I. J. Kramer, D. Zhitomirsky, A. G. Pattantyus-Abraham, L. Levina, L. Etgar, M. Grätzel, E. H. Sargent, *Adv. Mater.* **2011**, *23*, 3134–3138.

[9] A. Pivrikas, N. S. Sariciftci, G. Juška, R. Österbacka, *Prog. Photovoltaics* **2007**, *15*, 677–696.

[10] K. S. Leschkies, A. G. Jacobs, D. J. Norris, E. S. Aydil, *Appl. Phys. Lett.* **2009**, *95*, 193103.

[11] J. D. Bass, C. D. Schaper, C. T. Rettner, N. Arellano, F. H. Alharbi, R. D. Miller, H.-C. Kim, *ACS Nano* **2011**, *5*, 4065–4072.

[12] P. R. Brown, R. R. Lunt, N. Zhao, T. P. Osedach, D. D. Wanger, L.-Y. Chang, M. G. Bawendi, V. Bulović, *Nano Lett.* **2011**, *11*, 2955–2961.

[13] J. Gao, C. L. Perkins, J. M. Luther, M. C. Hanna, H.-Y. Chen, O. E. Semonin, A. J. Nozik, R. J. Ellingson, M. C. Beard, *Nano Lett.* **2011**, *11*, 3263–3266.

[14] H. Liu, J. Tang, I. J. Kramer, R. Debnath, G. I. Koleilat, X. Wang, A. Fisher, R. Li, L. Brzozowski, L. Levina, E. H. Sargent, *Adv. Mater.* **2011**, *23*, 3832–3837.

[15] O.-H. Park, J. Y. Cheng, H. S. Kim, P. M. Rice, T. Topuria, R. D. Miller, H.-C. Kim, *Appl. Phys. Lett.* **2007**, *90*, 233102.

[16] W. E. Spicer, *J. Vacuum Sci. Technol.* **1979**, *16*, 1422.

[17] P. Nagpal, V. I. Klimov, *Nat. Commun.* **2011**, *2*, 486.

[18] Y. G. Lee, C. G. Kang, U. J. Jung, J. J. Kim, H. J. Hwang, H.-J. Chung, S. Seo, R. Choi, B. H. Lee, *Appl. Phys. Lett.* **2011**, *98*, 183508.

[19] J. van de Lagemaat, N.-G. Park, A. J. Frank, *J. Phys. Chem. B* **2000**, *104*, 2044–2052.

[20] D. Zhitomirsky, I. J. Kramer, A. J. Labelle, A. Fischer, R. Debnath, J. Pan, O. M. Bakr, E. H. Sargent, *Nano Lett.* **2012**.

[21] I. J. Kramer, E. H. Sargent, *ACS Nano* **2011**, *5*, 8506–8514.

[22] Z. Fan, H. Razavi, J.-won Do, A. Moriwaki, O. Ergen, Y.-L. Chueh, P. W. Leu, J. C. Ho, T. Takahashi, L. A. Reichertz, S. Neale, K. Yu, M. Wu, J. W. Ager, A. Javey, *Nat. Mater.* **2009**, *8*, 648–653.

[23] M. A. Hines, G. D. Scholes, *Adv. Mater.* **2003**, *15*, 1844–1849.

COMMUNICATION